Inter- and intramolecular hydrogen bond in methyl 2-hydroxy-9H-1-carbazole carboxylate: Effect of solvents and acid concentration

ARTICLE *in* JOURNAL OF PHOTOCHEMISTRY AND PHOTOBIOLOGY A CHEMISTRY · JANUARY 2004

Impact Factor: 2.5 · DOI: 10.1016/S1010-6030(03)00350-2

2 AUTHORS:

Manoj Kumar Nayak
Council of Scientific and Industrial Researc…
25 PUBLICATIONS **217** CITATIONS
SEE PROFILE

S. K. Dogra
Indian Institute of Technology Kanpur
129 PUBLICATIONS **2,201** CITATIONS
SEE PROFILE

Available online at www.sciencedirect.com
SCIENCE DIRECT®
Journal of Photochemistry and Photobiology A: Chemistry 161 (2004) 169–183
Journal of Photochemistry and Photobiology A:Chemistry
www.elsevier.com/locate/jphotochem

Inter- and intramolecular hydrogen bond in methyl 2-hydroxy-9H-1-carbazole carboxylate: effect of solvents and acid concentration

Manoj K. Nayak, Sneh K. Dogra*

Department of Chemistry, Indian Institute of Technology Kanpur, Kanpur 208016, India

Received 7 May 2003; accepted 4 June 2003

Abstract

The photo-physics of methyl 2-hydroxy-9H-1-carbazazole carboxylate (MPCC) in different solvents and cyclohexane-trifluoroethanol (TFE) mixtures has been studied by means of absorption, fluorescence, fluorescence excitation spectra, time dependence spectrofluoremetery and AM1 semi-empirical quantum mechanical calculations. Only one small Stoke's shifted fluorescence band is observed under all the environments, indicating that the geometry of the molecule is not changed much on excitation to the first singlet state (S_1) and excited state intramolecular proton transfer (ESIPT) is not viable both in the ground (S_0) and S_1 states at the room temperature. AM1 calculation shows that the ESIPT is still endothermic in S_1 state. Single exponential decay is observed in the fluorescence from MPCC in all the solvents except acetonitrile and methanol. This suggests that in these two solvents, at least two different conformers are present in the S_0 state, whose absorption spectra are not different from each other. Spectral characteristics of MPCC in cyclohexane as a function of TFE have shown a slight blue shift in the λ^{ab}_{max}, decrease in the ε_{max}, red shift in the λ^{fl}_{max} and decrease in the ϕ_{fl}. This suggests that intermolecular hydrogen bonding is playing a major role in the deactivation of the fluorescence intensity than the intramoleuclar hydrogen bonding (IHB). Spectral properties of MPCC were also studied as a function of acid–base concentrations. pK_a values for different prototropic equilibriums were determined in S_0 and S_1 states and discussed.

Keywords: Methyl 2-hydroxy-9H-1-carbazazole carboxylate (MPCC); Intramoleuclar hydrogen bonding; Singlet state

1. Introduction

Proton transfer, especially intramolecular in the singlet state (S_1) state has received a lot of attention in recent times [1–13], but still it is not as understood as the proton transfer reaction in the ground state (S_0) from both a practical and fundamental perspective [14–16]. Excited state intramolecular proton transfer (ESIPT) reaction has centered on the transfer of a proton across the intramoleuclar hydrogen bonding (IHB). Molecules in which absorption occurs at much shorter wavelength (SW) than fluorescence that follows the proton transfer, resulting in a large Stoke's shift in the fluorescence spectrum, have found lot of interest. The reason being that these molecules have found a number of diverse applications, e.g. lasers [17–19], energy/data storage devices and optical switching [20,21], Raman filters and hard-scintillation counters [22], polymer photo-stabilizers [23–25] and triplet quenchers [26,27]. Photo biologists have suggested that ESIPT reactions can be used in understanding the binding properties of proteins [28,29], as well as, ESIPT can be used as fluorescence probes for bio-molecules [30,31].

It is well understood that the main conditions for the ESIPT to occur are the presence of IHB between the acidic centers (–OH, $–NH_2$ groups) and the basic centers (> C=O, =N– groups) in the S_0 state and the presence of proper energy levels of the enol and keto forms in the S_1 state. The driving force behind the ESIPT is the increase in the acidity and basicity of the respective acidic and basic centers up on excitation. Thus, main features common to many ESIPT reactions are their rapidity on the sub-pico second time scale [9,32] and this has been attributed to a barrier less process or at least with very low barrier [33,34].

Our laboratory has been active in synthesizing and studying the photo-physics of those molecules showing ESIPT behavior [35–37]. In all these molecules, the acidic centers have been either –OH group or $–NH_2$ group, but the basic center has been only =N– moiety. In all these molecules, respective rotamers were present in the S_0 state to give

* Corresponding author. Tel.: +91-512-597163; fax: +91-512-590007.
E-mail address: skdogra@iitk.ac.in (S.K. Dogra).

1010-6030/$ – see front matter © 2004 Elsevier B.V. All rights reserved.
doi:10.1016/S1010-6030(03)00350-2

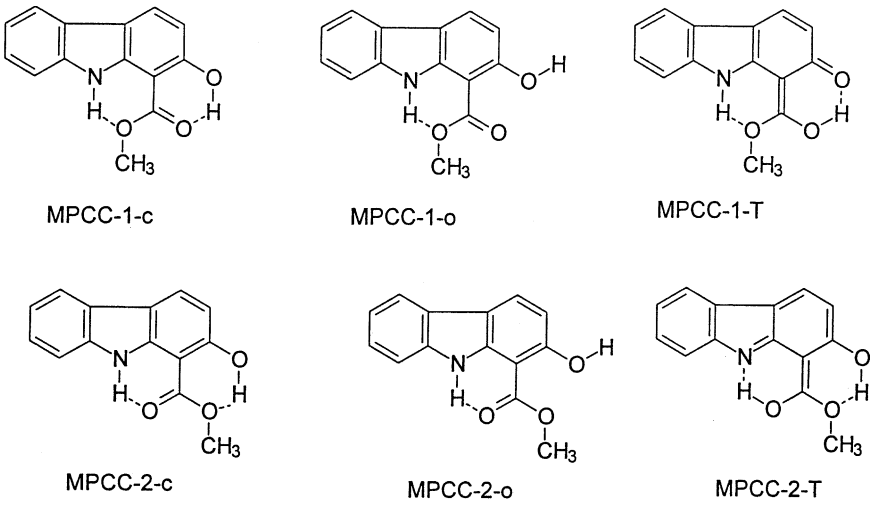

Scheme 1.

rise to either small Stokes shifted normal emission or the large Stokes shifted tautomer emission or both. Further, the presence of single fluorescence band either from the enol form or from keto form or the dual emission from both the forms depend on: (i) changes in the pK_a values of the acidic and the basic centers on excitation to S_1 state [38]; (ii) energy gap between the enol and the keto forms in the S_1 state and; (iii) the presence of different conformers leading to or not leading to enol one. Thus it is important to note that the presence of IHB between the acidic and the basic centers in a molecule do not guarantee that ESIPT will occur. For example, the molecule like 1-aminoanthraquinone [39], 1,4-dihydroxyanthraquinone [40,41] and I-hydroxy-9-fluorenone [42] (1-HF), do not exhibit evidence of a large Stokes shifted emission (i.e. the tautomer band). As suggested, the energetic factors inhibit the ESIPT in these molecules.

The present study involves the spectroscopic study of methyl 2-hydroxy-9H-1-carbazazole carboxylate (MPCC). The beauty of this molecule is that it has two acidic centers (–OH, > N–H groups) which can form IHB with basic center > C=O group in the S_0 state (i.e. MPCC-1 and MPCC-2, Scheme 1) and in principle this molecule can lead to the formation of two tautomers by ESIPT process. Thus, we have studied the photo-physics of this molecule using absorption, fluorescence excitation, fluorescence spectra and time dependence fluorimetry. We have also carried out the AM1 semi-empirical quantum mechanical calculations to confirm the formation of the desired species. Further, we have also studied the effect of acid–base concentrations on the spectral characteristics of MPCC. pK_a values for different prototropic reactions of MPCC are determined and discussed.

2. Materials and methods

Sodium salt of 2-hydroxy-9H-1-cabazole carboxylic acid was procured from Aldrich, UK, whereas the ester (MPCC) of the above acid was prepared by using dimethyl sulphate in acidic medium, as suggested in literature [43]. Both these compounds were purified by repeated crystallization from ethanol. Obtaining identical fluorescence and fluorescence excitation spectra with different excitation and emission wavelengths respectively in any one particular solvent checked the purity of both the compounds. All the solvents, except ethanol, were either of spectroscopic grade or HPLC grade from Merck and were used as such. Commercial ethanol was purified as described in literature [44]. Triply distilled water was used for the preparation of aqueous solutions.

The procedure to prepare the solutions and adjustment of pH was the same as mentioned in our recent paper [45]. The absorption spectra were recorded on a Shimadzu UV-Vis spectrophotometer equipped with a 135U chart recorder. Steady state fluorescence and fluorescence excitation spectra were recorded on a Fluorolog-3 (ISA Jobin Spex Instruments S.A. Inc.) spectrofluorimeter and all the spectra reported were corrected ones. The bandwidth used for recording the fluorescence and fluorescence excitation spectra were 2 and 3 nm, respectively. Lifetimes in different solutions were measured on a nanosecond single-photon counting spectrofluorimeter (PS 70/80) supplied by Applied Photo-physics, England. The electronic processing equipment and multi-channel analyzer were from Ortec and Norland, respectively. Nitrogen gas was used in the flash lamp. The flash lamp profile, defined by the full width at half the maximum height (FWHM) is 2 ns at the lamp frequency of 30 kHz. The fluorescence decay was analyzed by the re-convolution technique (software provided by IBH consultants, UK). The computer used was an IBM-based AT386. The lifetimes so reported possess the χ^2 in the range of 1 ± 0.2 and good auto-correlation functions. The error involved in the measurements of emission lifetime, taking into account the experimental facts is 10% and 0.2 ns is the shortest lifetime which can be measured under the best conditions of the experiments. The fluorescence quantum

yields (ϕ_{fl}) have been calculated from the solutions having absorbance less than 0.1, using quinine sulphate in 1 N H_2SO_4 as reference ($\phi_{fl} = 0.55$) [46]. The concentration of MPCC was kept at 1×10^{-5} M.

3. Semi-empirical quantum mechanical calculations

MPCC can be represented by two rotamers, i.e. MPCC-1, where the hydroxyl group is intramolecularly hydrogen bonded to carbonyl group and MPCC-2, where ≻NH proton is intramolecularly hydrogen bonded to the carbonyl group. Each rotamer can be represented as closed forms (MPCC-1-c, MPCC-2-c), open forms (MPCC-1-o, MPCC-2-o) and tautomer forms (MPCC-1-T, MPCC-2-T), where the hydroxyl or ≻NH protons are intramolecularly transferred to carbonyl group along with the structural reorientation. These species are given in Scheme 1. PCMODEL program [47] was used to find the initial geometry of each species. This program helped us to draw the structure of each species, optimized roughly the geometry using MM2 force field and generates the corresponding coordinates. Using these coordinates, the ground state geometry of all the species were then optimized using AM1 method (QCMP137, MOPAC 6/PC) [48]. As suggested and found by others [45,49–53], this method provides acceptable approximations to give results, which are quite close to the experimental finding. Total energy (E), dipole moment (μ), and dihedral angle (φ) have been compiled in Table 1. The geometry of the desired species was also optimized in the S_1 state using MOPAC program and by keeping the coordinates same as in the S_0 state. This procedure is also known as "Single Point Calculations". The values of energies so obtained represent the Franck–Condon states and thus can be used to calculate the transitions energies for the vertical transitions. These parameters are represented by the single prime in Table 1. Similar calculations were also performed taking into account CI (CI = 5 in MOPAC, total configurations 100). Each species was also fully optimized in the S_1 state using the above program with CI and without any constraint. The molecular parameters for each species were also calculated exactly in the similar manner in the S_0 state as done for each species by keeping the excited state coordinates and are represented by double prime in Table 1.

Dipolar solvation energies for different species have been calculated using the following expression based on Onsager's theory [54,55]

$$\Delta E_{solv} = -\left(\frac{\mu^2}{a^3}\right) f(D) \quad (1)$$

where $f(D) = (D-1)/(2D+1)$, D is the dielectric constant of the solvent, μ the dipole moment of the fluorophore in the respective state and a is the Onsager's cavity radius. For non-spherical molecule like MPCC, the value of a have been obtained by taking the 40% of the maximum length of the molecule [56]. The maximum length of the molecule was obtained from the optimized geometry of MPCC. The value of a obtained for MPCC is 0.4 nm. It may be mentioned here that we have not taken into account the specific interactions like hydrogen bonding with the solvents, etc. for the calculation of total energies. The total energies including solvation energy for each species in water are compiled in Table 1. The absorption and fluorescence transitions obtained theoretically and experimentally are compiled in Table 2.

Relative stability of each rotamer has been obtained by presetting the dihedral angle between the hydroxyl group and the carbonyl group (MPCC-1-c to MPCC-1-o), hydroxyl group and methoxy group (MPCC-2-c to MPCC-2-o) and between the ester group and the carbazole moiety (MPCC-1-c to MPCC-2-c) and then fully optimizing all

Table 1
Calculated parameters for the different rotamers/tautomers of MPCC

	MPCC-1-c	MPCC-1-o	MPCC-1-T	MPCC-2-c	MPCC-2-o	MPCC-2-T
Ground state						
$-E$ (eV)	3111.4875	3111.2544	3110.6665	3111.4759	3111.3284	3109.9656
$-E_{sol}$ (eV)	3111.5269	3111.2825	3110.7693	3111.4767	3111.3415	3110.0125
$-E''$ (eV)	3111.3746	3111.0048	3110.3092	3111.3308	3111.2795	3109.5270
$-E''_{sol}$ (eV)	3111.4141	3111.0251	3110.4330	3111.3318	3111.2925	3109.6069
μ (D)	2.84	2.47	4.47	0.5	2.0	3.74
μ'' (D)	2.84	2.1	4.9	0.35	2.0	4.88
φ_1	0.2	−30.0	0	169	176	−1.5
S_1 state						
$-E$ (eV)	3108.1045	3107.7412	3107.9236	3108.1043	3107.8616	3107.6101
$-E_{sol}$ (eV)	3108.2171	3107.7812	3108.1091	3108.1320	3107.8785	3107.6466
$-E'$ (eV)	3108.0404	3107.6943	3108.0360	3108.0360	3107.8136	3107.3193
$-E'_{sol}$ (eV)	3108.1329	3107.7430	3108.0515	3108.0458	3107.8327	3107.3240
μ (D)	4.8	2.95	6.0	2.9	2.27	3.3
μ' (D)	4.35	3.25	1.73	1.72	2.4	1.18
φ_1	1.4	−25.2	1.6	173.7	176	1.5

Double prime represents the parameters of the S_0 state obtained with S_1 state geometry. Single prime represents the parameters of the S_1 state with S_0 state geometry.

Table 2
Assignment of the excitation and fluorescence transitions of different species of MPCC in terms of calculated energies (eV) with and without solvation energies and the experimental values

Species	Excitation spectrum				Fluorescence spectrum			
	Without solvation		With solvation		Without solvation		With solvation	
	Single point	Experimental	Single point	Experimental	Single point	Experimental	Single point	Experimental
MPCC-1-c	3.45	3.41	3.39	3.48	3.27	3.14	3.20	3.07
MPCC-1-o	3.56		3.54		3.26		3.24	
MPCC-1-T	2.63		2.72		2.39		2.32	
MPCC-2-c	3.44		3.43		3.23		3.20	
MPCC-2-o	3.52		3.51		3.41		3.42	
MPCC-2-T	2.65		2.69		1.92		1.96	

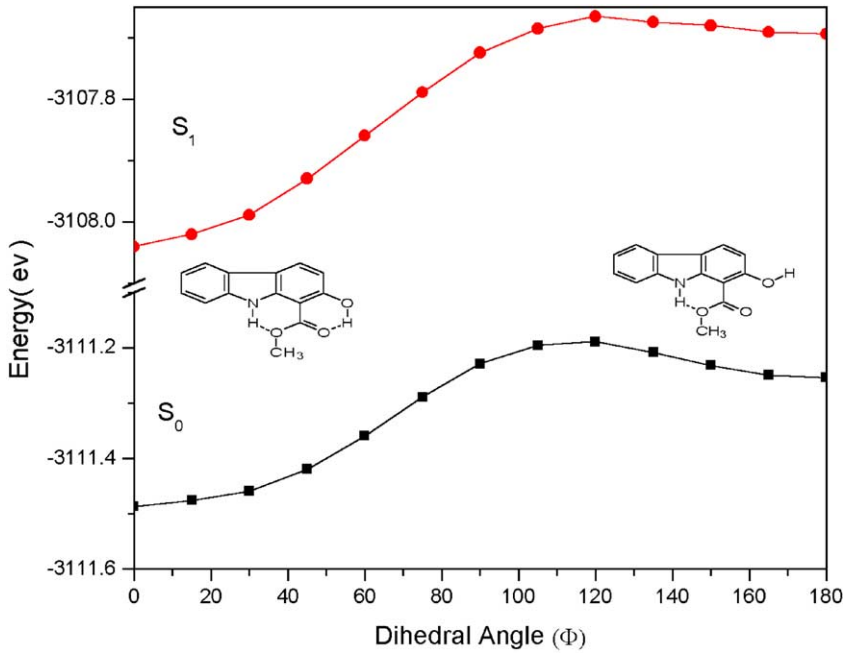

Fig. 1. Energetic of transformation of MPCC from MPCC-1-c to MPCC-1-o in S_0 and S_1 states as a function of dihedral angle.

the parameters. Energies so obtained for each rotamer are plotted in Figs. 1–3, respectively. These figures depict the interconversion of MPCC-1-c to MPCC-1-o, MPCC-2-c to MPCC-2-o and MPCC-1 to MPCC-2, respectively. Similarly, potential energy curves for the respective interconversion in the S_1 state were also obtained as the function of respective dihedral angle by adding the transition energies (ΔE_{ij}, calculated by the single point calculations) to the respective S_0 value (E_i). The values of minimum dihedral angles obtained from the minimum energy of the rotamers from the respective figures agree nicely with those obtained by optimization process.

The interconversion of MPCC-1-c to MPCC-1-T or MPCC-2-c to MPCC-2-T in the S_0 and S_1 states can be thought of as arising from proton transfer from hydroxyl group to carbonyl oxygen in the former or proton transfer from >N–H proton to carbonyl oxygen in the latter species with simultaneous distribution of charge in and around the six member hydrogen bonded ring. One can also consider it as hydrogen atom in both cases. In either case, one requires to identify the reaction coordinate and calculate the potential energy change along the reaction coordinate. We have varied the O–H (> N–H) distance and optimized the rest of the structural parameters to get the potential energy for each $r_{O–H}$ ($r_{>N–H}$) distance and plots are given in Figs. 4 and 5, respectively. Similar potential energy curves in the S_1 state were also obtained by the same procedure as followed above for the interconversion of the closed forms to the open forms and are shown in Figs. 4 and 5, respectively.

4. Results

4.1. Absorption spectrum

Fig. 6 depicts the absorption spectra of MPCC in some selected solvents and relevant data are compiled in Table 3. The absorption spectrum can be divided into three regions,

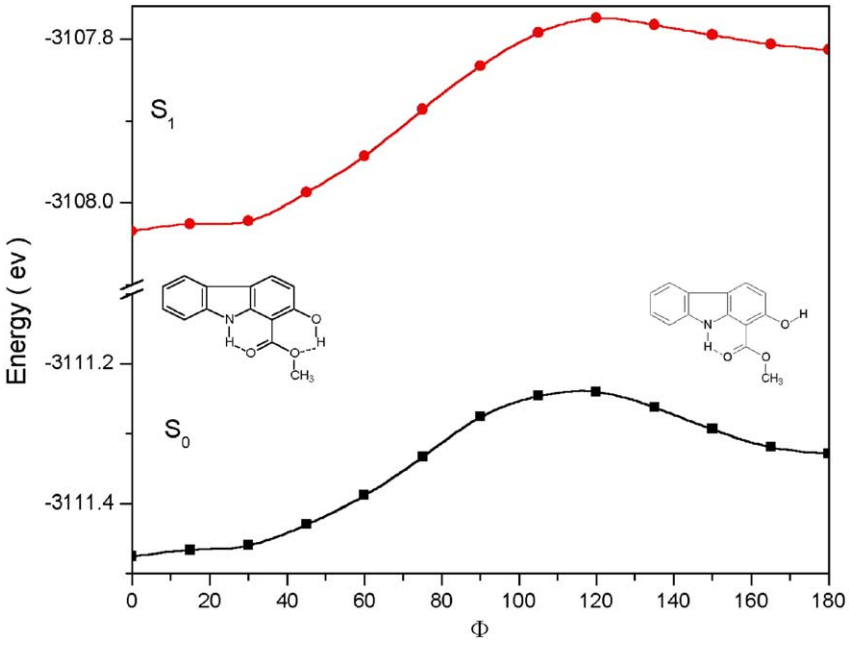

Fig. 2. Energetic of transformation of MPCC from MPCC-2-c to MPCC-2-o in S_0 and S_1 states as a function of dihedral angle.

long wavelength (LW) absorption band comprises the region >340 nm, the middle wavelength (MW) band is between 300 and 340 nm and the short wavelength absorption band is between 250 and 300 nm. LW and MW absorption spectra are structured in cylcohexane with vibrational frequency as ∼700 and ∼1200 cm^{-1}, respectively and the structure is destroyed in polar solvents. On the other hand, the SW absorption band is also structured ($\bar{\upsilon}_{vib}$ =∼ 750 cm^{-1}) and the structure is retained even in the most polar protic solvent like water. In other words, the LW and MW absorption band systems are influenced by the presence of substituents on carbazole and thus get affected by the changes in the environments, where as the SW absorption band is associated with the parent carbazole moiety. All the three band systems are blue shifted with increase in the polarity and hydrogen bond forming capacity of

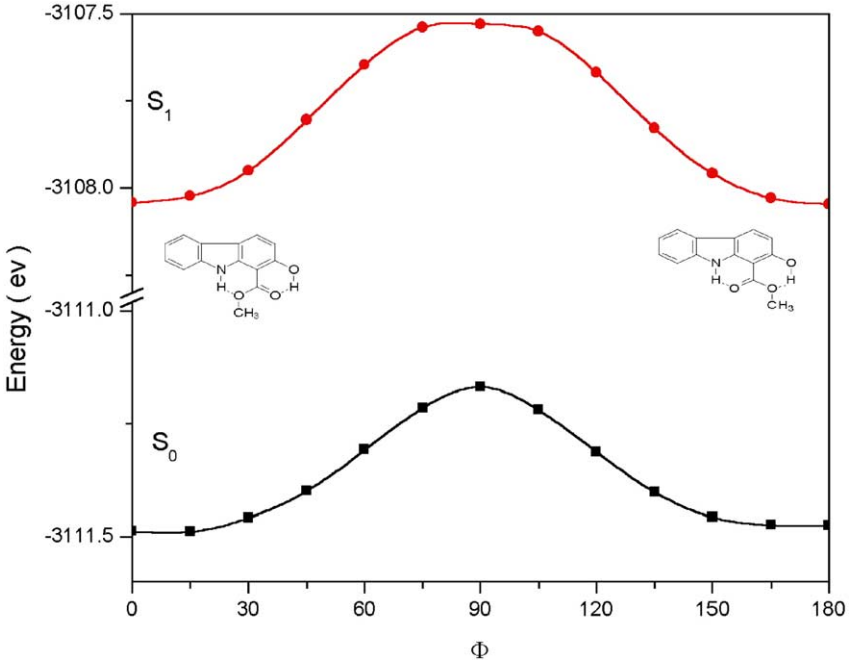

Fig. 3. Energetic of transformation of MPCC from MPCC-1-c to MPCC-2-c in S_0 and S_1 states as a function of dihedral angle.

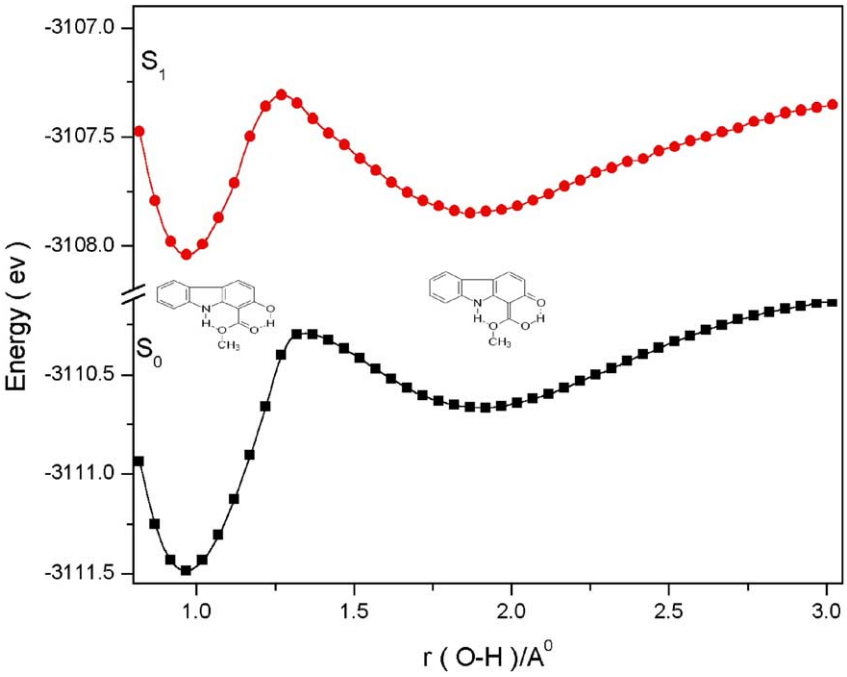

Fig. 4. Energetic of transformation of MPCC from MPCC-1-c to MPCC-1-T in S_0 and S_1 states as a function of $r_{O–H}$.

the solvents, but the maximum blue shift is observed in the LW absorption band under the similar environments. A slight decrease in the molecular extinction coefficient and increase in FWHM are notice under the similar set of solvents.

Infra-red absorption spectrum of MPCC has been recorded both in KBr pallet and CCl_4 solution and shown in Fig. 7. The lowering of O–H stretching frequency to 3390 cm^{-1} clearly suggests the presence of IHB between the carbonyl oxygen and hydroxyl proton.

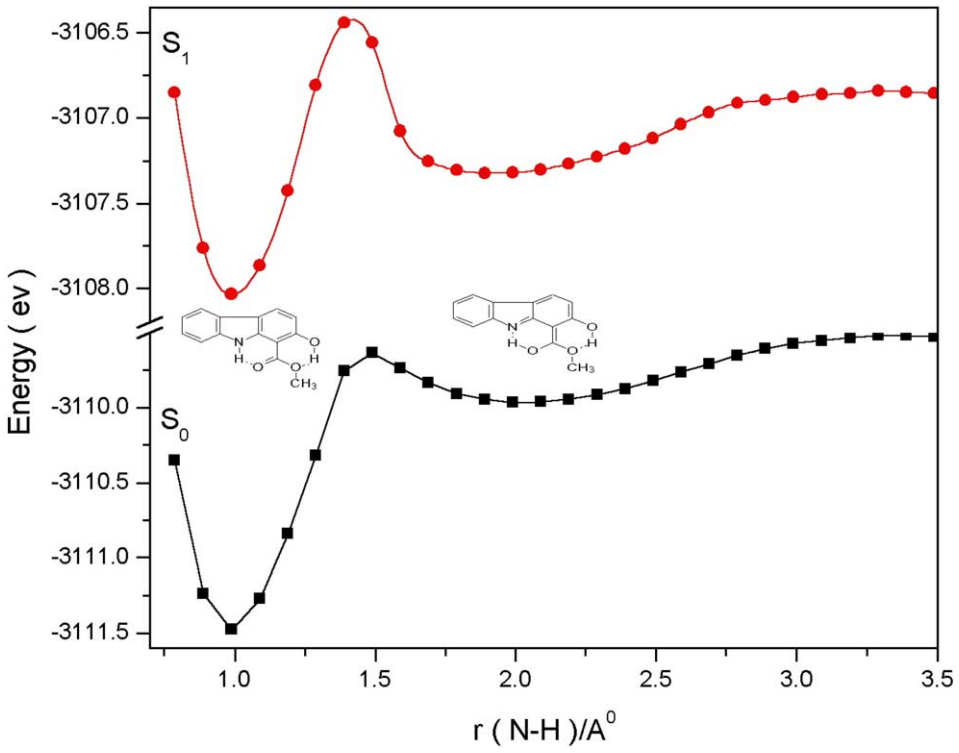

Fig. 5. Energetic of transformation of MPCC from MPCC-2-c to MPCC-2-T in S_0 and S_1 states as a function of $r_{N–H}$.

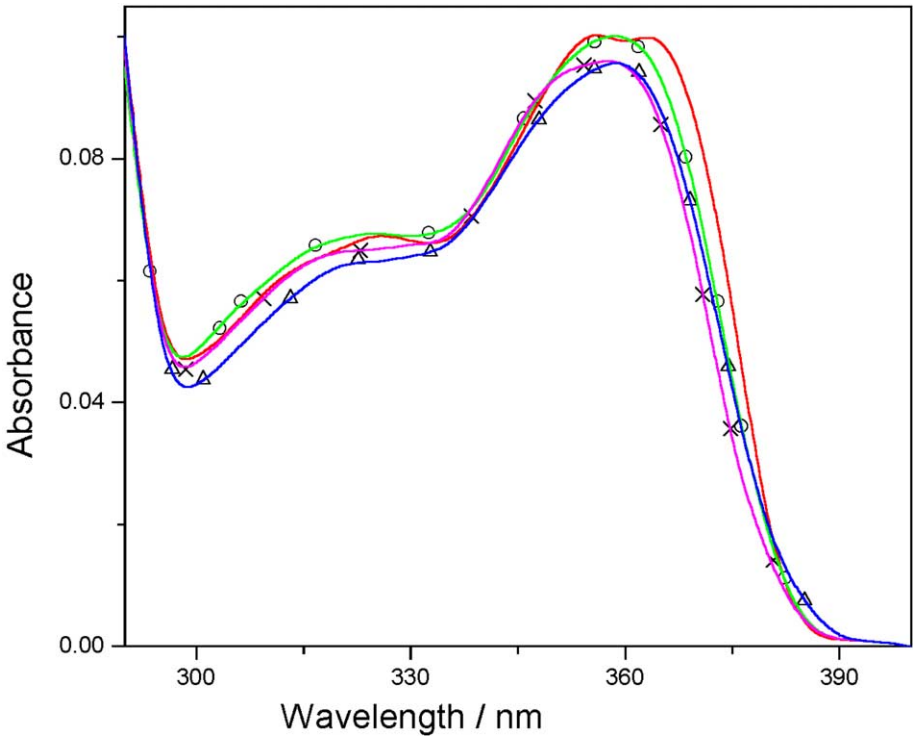

Fig. 6. Absorption spectrum of MPCC in some selected solvents. (—) cyclohexane; (○) dioxane, (×) acetonitrile; (△) methanol. [MPCC] = 1×10^{-5} M.

4.2. Fluorescence spectrum

Fig. 8 depicts the fluorescence spectrum of MPCC in some selected solvents and the relevant data are compiled in Table 4. Only one small Stokes shifted fluorescence band is observed in different solvents and at different excitation wavelengths (λ_{exc}). This band is very sensitive to the solvent polarity, suggesting that greater charge transfer takes place between the carbazole and the substituents in the S_1 state than in the S_0 state. A continuous red shift observed in the fluorescence band maximum (λ^{fl}_{max}) with increasing polarity and hydrogen bond forming tendency of the solvents, indicates the increase in the delocalization of the π cloud of the carboxylic group and the lone pair of the hydroxyl group throughout the carbazole moiety in the S_1 state. Fluorescence quantum yield (ϕ_{fl}) decreases under the similar environments. These results suggest the stronger interactions between the fluorophore and the solvents. Both λ^{fl}_{max} and ϕ_{fl} of MPCC are insensitive to the change in the λ_{exc}. This confirms that the fluorescence is occurring from the most relaxed first singlet state and is consistent with the fact that the solvation relaxation time of the solvents used is smaller than the lifetime of the fluorophore.

The fluorescence excitation spectra of MPCC in different solvents are recorded at different λ_{em} in the range of 380–500 nm. In each case, the fluorescence excitation spectra (not shown) resemble with each other and also with the absorption spectra in the respective solvent. This suggests that there is only one species for MPCC in the S_0 state.

The FWHM of the fluorescence band is nearly invariant in the polar aprotic solvents, but increases with increase in the hydrogen bond donor strength. FWHM of the LW

Table 3
Absorption band maximum (λ^{ab}_{max}, nm), molecular extinction coefficient ($\log \varepsilon$) and FWHM (cm^{-1}) of the long wavelength absorption band maximum of MPCC

Solvents	λ^{ab}_{max}						FWHM
1. Cyclohexane	280 (4.43)	286 (4.51)	313 (sh)	325 (3.83)	355 (4.0)	364 (4.0)	3340 (3290)
2. Ether	279 (4.43)	285 (4.46)	–	324 (3.83)	–	362 (4.0)	3390 3290
3. Dioxane	279 (4.41)	285 (4.43)	–	323 (3.83)	–	360 (3.99)	3400 (3360)
4. Ethyl acetate	278 (4.40)	284 (4.42)	–	322 (3.81)	–	360 (3.99)	3400 (3370)
5. Acetonitrile	278 (4.40)	284 (4.42)	–	322 (3.80)	–	360 (3.98)	3360 (3440)
6. Methanol	279 (4.38)	285 (4.40)	–	322 (3.79)	–	360 (3.98)	3400 (3570)
7. H_2O (saturated) (pH = 6.0)	279	282	–	320	–	356	3500 (3630)
8. H_2O/methanol (pH = 12.4)	280 (4.44)	288 (4.42)	313 (4.04)	325 (sh)	350 (4.01)	367 (3.94)	4470 (4460)
9. H_2O/methanol (H_- = −15.8)	280 (4.42)	–	–	327 (4.09)	346 (4.14)	–	5210 (4660)

[MPCC] = 1×10^{-5} M. Values of FWHM in parenthesis are of the LW excitation fluorescence spectrum.

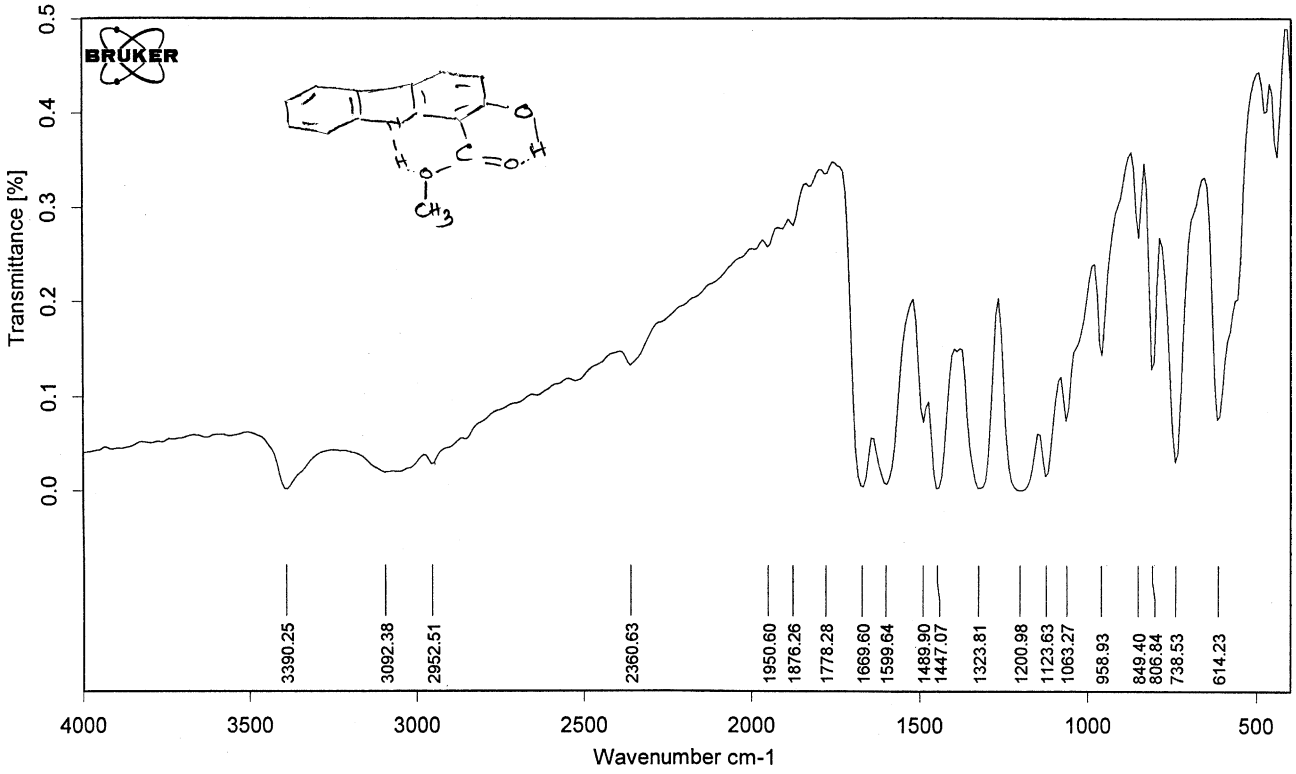

Fig. 7. Infra-red spectrum of MPCC, recorded in KBr pallet.

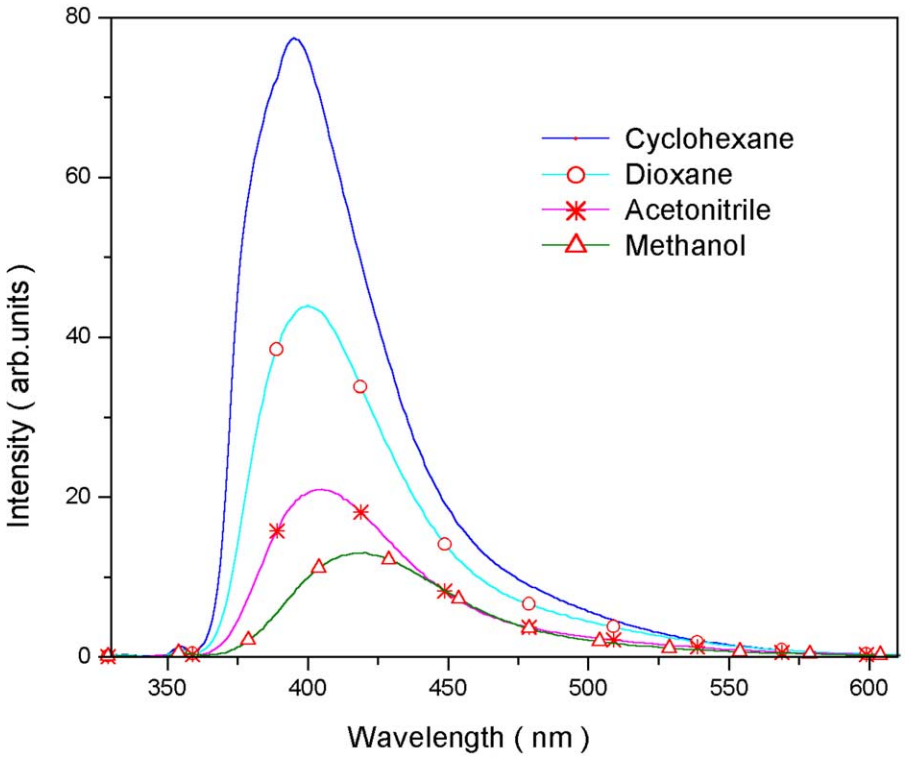

Fig. 8. Fluorescence spectrum of MPCC in some selected solvents. (—) cyclohexane; (○) dioxane, (×) acetonitrile; (△) methanol. [MPCC] = 1×10^{-5} M.

Table 4
Fluorescence band maximum (λ^{fl}_{max} (nm)), fluorescence quantum yield (ϕ_{fl}), FWHM (cm^{-1}), lifetime (τ (ns)), k_r ($10^{-7}\,s^{-1}$) and k_{nr} ($10^{-7}\,s^{-1}$)

Solvents	λ^{fl}_{max}	ϕ_{fl}	FWHM	τ	k_r	k_{nr}
1. Cyclohexane	395	0.253	3410	2.79	9.1	26.8
2. Ether	399	0.188	3440	2.32	8.1	35.0
3. Dioxane	400	0.157	3450	2.11	7.4	39.9
4. Ethyl acetate	401	0.138	3460	2.09	6.6	41.3
5. Acetonitrile	405	0.079	3480	0.96 (0.156), 2.97 (0.035)	5.8	67.0
6. Methanol	419	0.053	3710	0.48 (0.168), 4.13 (0.034)	4.6	82.4
7. Water (pH = 6)	434	0.048	3700	5.6	0.86	17.0
8. Water/methanol (pH = 12.4)	433	0.06	3630	0.45 (0.197), 6.35 (0.024)	–	–
9. Water/methanol (H_- = 15.8)	401	0.22	3390	1.94	11.3	40.0

[MPCC] = 1×10^{-5} M (λ_{exc} for lifetime = 354 nm and [MPCC] = 1×10^{-4} M).

absorption, as well as, that of LW fluorescence excitation band and the fluorescence band is nearly equal to each other in each solvent. This suggests that not much change is occurring in the geometry of the molecule on excitation to S_1 state. This is also reflected by the similar dihedral angle (φ) between the carbazole moiety and carboxylic ester group in S_0 and S_1 states (Table 1). Whatever changes are taking place in the spectral characteristics, are due to the solvent–solute interactions. This is reflected by the small Stokes shift (2160 cm^{-1}) observed in the cyclohexane as the solvent and decrease in the ϕ_{fl} in the polar protic solvents.

4.3. Lifetimes of the excited states

The excited state lifetimes of MPCC were measured in different solvents by using λ_{exc} = 354 nm, whereas the λ_{em} were the fluorescence band maxima in the respective solvent. The fluorescence intensity in each case, except acetonitrile and methanol, followed a single exponential decay with $\chi^2 = 1 \pm 0.1$ and with good auto-correlation functions. Fig. 9 represents a typical fluorescence decay profile of MPCC in acetonitrile. The decay of fluorescence intensities of MPCC in acetonitrile and methanol were also followed at λ_{em} = 360, 400 and 440 nm. The decay in each case followed a double exponential with $\chi^2 = 1 \pm 0.1$. The relative contribution of the amplitude of the short lifetime increases with the increase in the emission wavelength. This shows that there are two different kinds of species in these solvents. Species with shorter lifetime possesses the fluorescence band maximum towards the red side of the spectrum and that longer lifetime towards the shorter wavelength side. The values of radiative (k_r) and non-radiative (k_{nr}) rate

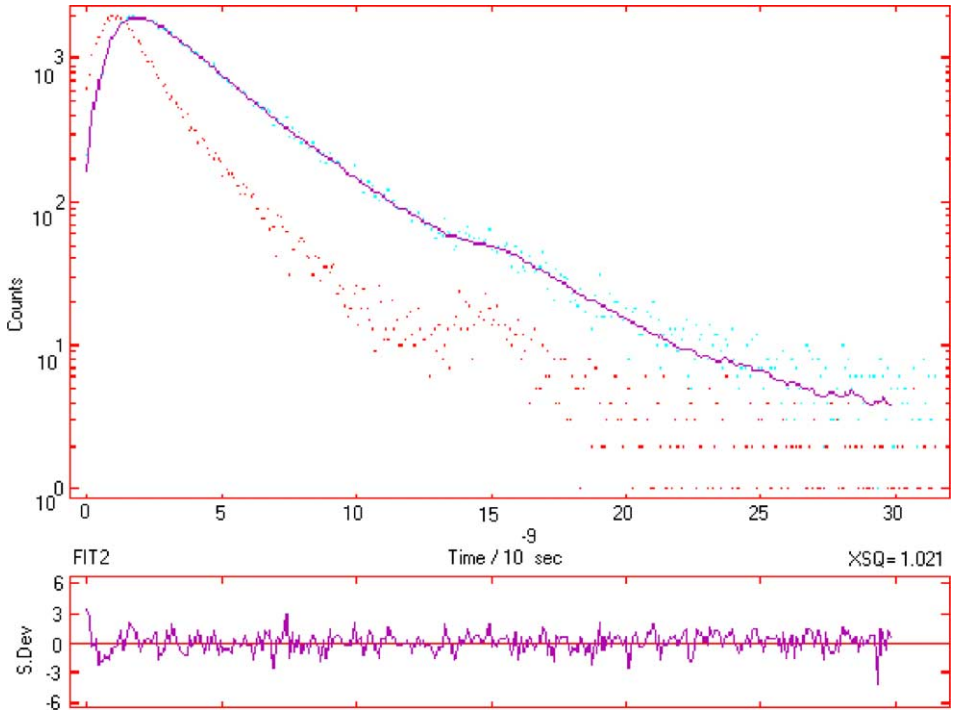

Fig. 9. Fluorescence decay curve of MPCC in acetonitrile. λ_{exc} = 354 nm; λ_{fl} = 405 nm. [MPCC] = 1×10^{-5} M.

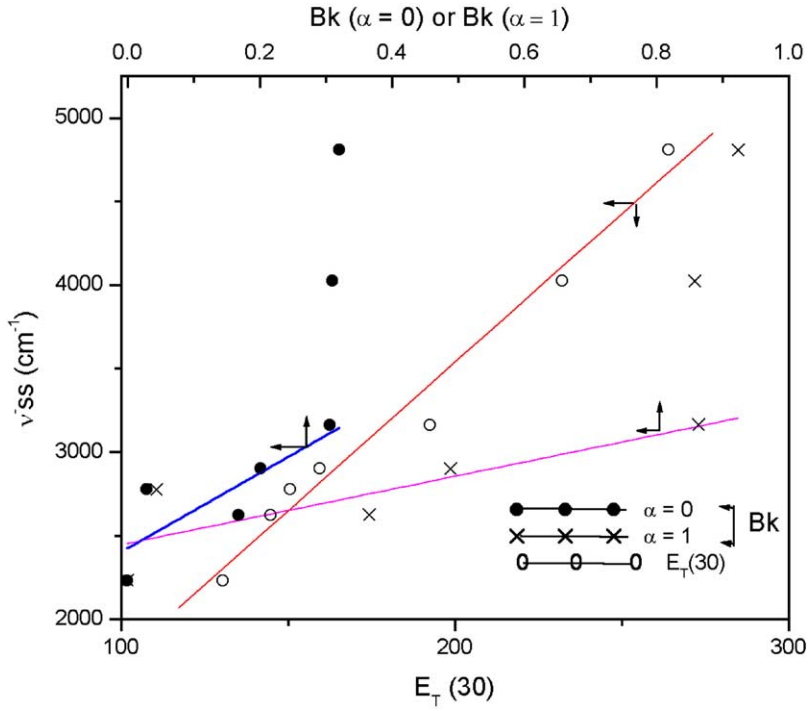

Fig. 10. Plot of Stokes shifts vs. BK parameters, $\alpha = 0$ and 1 and E_T (30) parameters. (●) $\alpha = 0$; (□) $\alpha = 1$; (○) E_T (30) parameter.

constants were calculated from the lifetimes (τ) and ϕ_{fl} using the following relations.

$$k_r = \frac{\phi_{fl}}{\tau}, \qquad k_{nr} = \left(\frac{1}{\tau}\right) - k_r$$

The values of k_r, k_{nr}, τ and ϕ_{fl} for MPCC in different solvents, except acetonitrile and methanol are compiled in Table 4. The values of k_r and k_{nr} in acetonitrile and methanol have been calculated using the average lifetime, obtained by taking into account the respective amplitude and lifetime. It is clear from the data of Table 4 that the values of k_{nr} increase with increase of the solvent polarity and their protic nature except water.

4.4. Dipole moments

The ground state dipole moments (μ_g) for the various species have been calculated using AM1 program after optimizing the geometry and are compiled in Table 1. Many equations are available to determine the excited state dipole moment (μ_e) from absorption and fluorescence data. We shall use the BK [57] Eq. (2) to calculate the μ_e. BK polarity parameters for $\alpha = 0$ and 1 (where α is the polarizability) have been taken from literature [57].

$$\bar{\upsilon}_{ab} - \bar{\upsilon}_{fl} = m_1 \left[\frac{D-1}{2D+1} - \frac{n^2-1}{2n^2+1}\right] + \text{constant} \qquad (2)$$

where

$$m_1 = \frac{(\mu_e - \mu_g)^2}{\beta a^3} \qquad (3)$$

$\beta = 2\pi\varepsilon_0 hc = 1.105 \times 10^{-35} C^2$. In case of isotropic polarizability (α) of the molecules, the condition $2\alpha/4\pi\varepsilon_0 a^3 = 1$ is frequently satisfied and Eq. (2) will represent BK equation. When the polarizability of the molecule is neglected, Eq. (2) reduces to Eq. (4), derived by Lippert [58] and Mataga et al. [59].

$$\bar{\upsilon}_{ab} - \bar{\upsilon}_{fl} = m_1 \left[\frac{D-1}{2D+1} - \frac{n^2-1}{2n^2+2}\right] + \text{constant} \qquad (4)$$

Fig. 10 presents plots of Stokes shifts versus BK parameters when $\alpha = 0$, Eq. (4) and when $\alpha = 1$, Eq. (2). A plot of Stokes shifts versus E_T (30) parameters is also included in Fig. 10. It is evident from Fig. 10 that the Stokes shifts observed in protic solvents is much larger than that expected on the basis of linear relations. The large deviation from linearity shown by protic solvent is due to the fact that hydrogen bond between the solvent and the lone pair of the hydroxyl group in the S_0 state is broken and hydrogen bond is formed between the hydroxyl proton and the lone pair of the solvent molecule. Because of this a large red shift is observed in the fluorescence spectra of MPCC. This is also reflected by the fact that hydroxyl group becomes stronger acid in the S_1 [38]. It is supported by the fact that the plot of Stokes shifts versus E_T

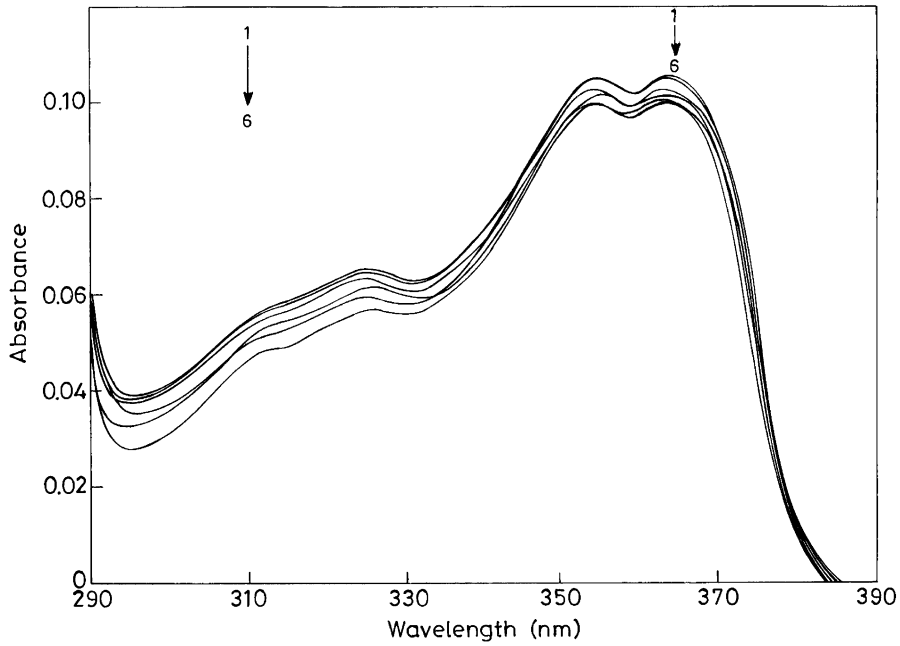

Fig. 11. Absorption spectrum of MPCC in cyclohexane at room temperature as a function of added concentration of TFE. [MPCC] = 1×10^{-5} M. (1) TFE = 0 M; (2) TFE = 1.39×10^{-3} M; (3) TFE = 6.95×10^{-3} M; (4) TFE = 1.39×10^{-2} M; (5) TFE = 6.95×10^{-2} M; (6) 1.39×10^{-1} M.

(30) parameter (Fig. 10), which also includes the specific interactions, is linear in all the solvents with regression coefficient (R) as 0.99. The peculiar properties of dioxane as a solvent are well known and the large deviations from linearity observed in this solvent can be explained on the same lines as made by Ledger and Supan [60]. $\Delta\mu_e$ was determined from the slope of the linear parts of the plots of Fig. 10 ($R = 0.98$ for both $\alpha = 0$ and $= 1$ and neglecting the protic solvents) and taking Onsager's cavity radius 'a' as 0.4 nm. The values of $\Delta\mu_e$ are found to be 3.9 D, for $\alpha = 0$, and 2.9 D for $\alpha = 1$ from the BK equations.

4.5. Effect of TFE

The absorption spectrum of MPCC was also recorded in cylcohexane containing trifluoroethanol (TFE) up to 0.139 M. The LW and MW absorption bands are shown in Fig. 11. A slight blue shift and decrease in ε_{max} of all the absorption band maxima are observed with increase in the TFE concentration. These results are similar to those observed in other protic solvents but are different from those noticed in 1-HF [42] and 1-amino-9-fluorenone (1-AF) [61]. λ^{fl}_{max} is red shifted from 395 to 404 nm, ϕ_{fl} decreases and FWHM increases from 3520 to 3870 cm^{-1} (Fig. 12) with the increase in the concentration of TFE in cyclohexane. Above-mentioned parameters remain invariant with the change in the λ_{exc}. These results are different from those observed in case of 1-HF [42] and 1-AF [61] in the sense that ϕ_{fl} for these molecules increase with increase in the TFE in cyclohexane.

4.6. Effect of acid–base concentrations

Effect of acid–base concentrations in the range of (H_0/pH/H_-) −10 to 16 on the absorption and fluorescence spectra of MPCC has also been studied in 30% (v/v) methanol/water mixture. In the basic solution at pH 12.4, the absorption spectrum of MPCC was red shifted (367 nm) in comparison to the neutral MPCC and is assigned to monoanion (MA) formed by deprotonating the hydroxyl group [38]. This is because the pK_a value for the deprotonation of aromatic alcohols falls in this range. On further increase in the base strength, the absorption spectrum of MPCC at H_- 15.8 gets blue shifted (346 nm) in comparison to both neutral and MA species. This has been assigned to the dianion (DA) obtained by further deprotonating the > N–H group of MA. On increasing acid concentration, the LW absorption band of MPCC starts red shifting (380 nm) at H_0 –0.72 and reached maximum value at H_0 –4.72. The LW absorption band (380 nm) is very broad as compared to that of neutral species (356). On the other hand, 280 nm absorption band of neutral species is red shifted only by 8 nm under the similar environments. Thus, these changes could be due to the formation of monocation (MC) obtained by protonating the > C=O group, as similar changes have also been observed in other similar systems [38]. Similar changes in the absorption spectrum (356 nm band with a tail towards red) of MPCC in cyclohexane containing 1 M trifluoroacetic acid (TFA) are very small. On further increase of acid concentration by adding H_2SO_4, the solution turns blue and LW absorption band becomes broad and diffuse, whereas no changes are observed in the 280 nm band system.

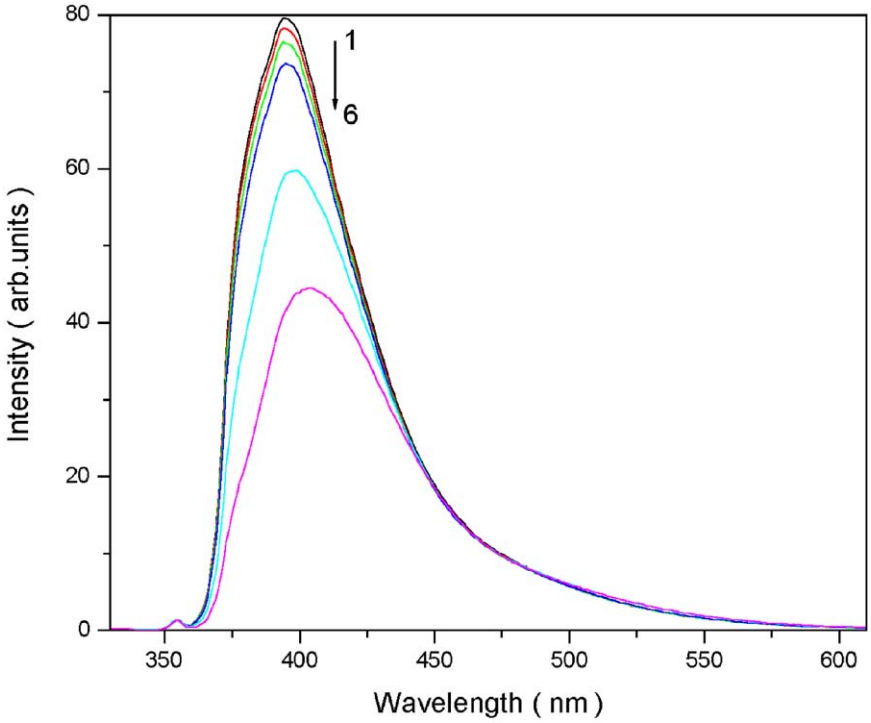

Fig. 12. Fluorescence spectrum of MPCC in cyclohexane at room temperature as a function of added concentration of TFE. [MPCC] = 1×10^{-5} M. (1) TFE = 0 M; (2) TFE = 1.39×10^{-3} M; (3) TFE = 6.95×10^{-3} M; (4) TFE = 1.39×10^{-2} M, (5) TFE = 6.95×10^{-2} M; (6) TFE = 0.139 M.

The absorption data were used to calculate the equilibrium constants for the MC–N, N–MA and MA–DA equilibria in the S_0 state. The pK_a values for the N–MA and MA–DA are found to be 10.2 and 14.4, respectively. The similar value for the MC–N equilibrium could not be calculated accurately but can be assigned the value of -5.2 ± 0.5. Similar value is also observed for other carbonyl protonation [38].

Fluorescence spectra of various species were recorded by exciting the samples at 312, 340, 360 and 365 nm. 340 and 365 nm, the isosbestic wavelengths for the N–MA and 312 and 360 nm are the isosbestic wavelengths for MA–DA equilibrium, respectively. The fluorescence band maximum and FWHM of MPCC at pH 12.40 (MA) is hardly affected by changing the λ_{exc}. The fluorescence band maximum of the MA is nearly similar to that of the neutral species, whereas the ϕ_{fl} of MA is invariant at λ_{exc} at 312 and 340 nm, but starts decreasing at λ_{exc} >340 nm. On the other hand, λ_{max}^{fl}, ϕ_{fl} and FWHM of MPCC at H_ 15.8 (i.e. DA) are independent of λ_{exc}. Under the acidic conditions, a new red shifted fluorescence band of very low intensity starts appearing at the expanse of neutral species of MPCC. Based on the earlier results [38], new emission can be assigned to the MC, formed by protonating the carbonyl group. With further increase of acid concentration, the fluorescence intensity is completely quenched. Thus, suggesting that proton-induced fluorescence quenching is observed [62]. Excited state pK_a (pK_a^*) values for all the three equilibriums were studied with the help of fluorometric titration method. Results indicate the observation of the ground state pK_a values for the N–MA and MA–DA equilibriums and 2.3 for the MC–N equilibrium from the fluorimetric titrations.

5. Discussions

Six possible species can be written for MPCC, as depicted in Scheme 1. From the data of Table 1 and Figs. 4 and 5, it is evident that MPCC-1-T and MPCC-2-T are unstable with respect to MPCC-1-c and MPCC-2-c by 79.3 and 145.8 kJ mol^{-1}, respectively, under isolated conditions in S_0 state. Taking into consideration even the dipolar solvation energy, although this instability reduces to 73.1 and 141.2 kJ mol^{-1}, respectively, still it is too high for these species to be present in S_0 state. The reduction in the instability of the two tautomers is because μ_g of each tautomer is larger than the respective enol structure. Further, the barrier height for the conversion of MPCC-1-c (or MPCC-2-c) to MPCC-1-T (or MPCC-2-T) is 114.7 kJ mol^{-1} (177.4 kJ mol^{-1}) and is very large in the S_0 state. This suggests that the intramolecular proton transfer in the S_0 state is unviable under the thermal conditions for both the species. In other words, MPCC-1-T and MPCC-2-T are not present in the S_0 state.

Under isolated conditions, both the closed forms of MPCC (MPCC-1-c and MPCC-2-c) are of nearly equal stability. The stability of MPCC-2-c increases by 4.9 kJ mol^{-1} as compared to MPCC-1-c, when solvation energy is taken into account. The barrier height for interconversion

of MPCC-1-c to MPCC-2-c is 30.9 kJ mol^{-1} in the S_0 state. On the other hand, both the open forms of MPCC (MPCC-1-o and MPCC-2-o) are unstable by 22.5 (Fig. 1) and 14.3 kJ mol^{-1} (Fig. 2) as compared to their respective closed forms and their instability further increases when dipolar solvation energies are taken into account. In other words, it may be mentioned here that only closed forms of MPCC are present in the system. These are further substantiated from the following results. Data of Table 2 indicate that with in the approximations used in these calculations, the agreement between the absorption and emission transitions predicted by single point calculations for the closed forms and those observed experimentally is very good under isolated conditions and when solvation energy is taken into account. This agreement is also good for the absorption spectrum when the results are compared even in water as solvent but the agreement becomes bad for the emission spectrum. This is obvious, as we have not taken in to account the hydrogen bonding interaction. This also confirms that the IHB is stronger in the S_1 state as compared to that in the S_0 state. Figs. 1 and 2 also reflect this because IHB increases from 22.5 to 33.4 kJ mol^{-1} in case of MPCC-1-c and from 14.1 to 21.4 kJ mol^{-1} in case of MPCC-2-c in the S_1.The barrier heights for the interconversion of MPCC-1-c to MPCC-1-o and MPCC-2-c to MPCC-2-o also increases from 28.7 to 36.2 kJ mol^{-1} in former and from 23.7 to 25.1 kJ mol^{-1} in S_1 state and thus their interconversion will also be slowed down in the S_1 state. This is reflected by the double exponential decay observed in the fluorescence intensity of MPCC in acetonitrile and methanol. This also suggests that the equilibrium between the open and closed structures is not established in the S_1 state.

Having established that only the closed forms of MPCC are present under isolated conditions, the experimental results can be discussed in the light of these observations. Molecular extinction coefficients, ϕ_{fl} and theoretical calculations confirm that all the transitions observed are of $\pi\pi^*$ in nature. Further, it has also been shown [63] that 343 nm absorption band of carbazole moiety is short axis polarized and the 295 and 265 nm bands are long axis polarized. Thus, the presence of substituents along the shorter axis will affect the LW transition and their presence along the longer axis will affect the second and third bands. Hardly any changes observed in the LW band in 2-hydroxycarbazole [64] confirm this. In other words, a large red shift observed in 343 nm absorption band of carbazole moiety in MPCC confirms the planarity of the ester group and hydroxyl lone pairs (Table 1). The decrease in the sensitivity of absorption bands towards solvents as one moves towards the blue side of the spectra support the above argument. This suggests that the LW absorption band of the carbazole moiety is influenced more by the presence of IHB between the substituents and ≻N–H group as shown in the Scheme 1. The blue shift observed with the increase in the solvent polarity and hydrogen bonding capacity favors the formation of open structures. Thereby losing the co-planarity of the ester group with the carbazole moiety. This will be also reflected later. Increase in the FWHM of the absorption spectrum in polar protic solvents also substantiates this.

Very small Stokes shift observed in the fluorescence spectrum of MPCC in cyclohexane, only 2150 cm^{-1}, confirms that the emission is observed from the normal species and not from the tautomer. This also suggests that the geometry of the molecule does not change much on excitation to S_1 state. Large red shift in the fluorescence band maximum reflects the greater delocalization of the π cloud of the ester group and the lone pair of the hydroxyl oxygen with the carbazole moiety. The total energy data of Table 1 show that both the open structures of MPCC are not favorable under isolated and solvated conditions. Solvatochromic results have further confirmed the above observation. This is because the AM1 calculations have shown that $\Delta\mu$ on excitation to S_1 state are only 0.5 and 0.25 D in MPCC-1-o and MPCC-2-o respectively, whereas the $\Delta\mu$ observed from the BK plot with $\alpha = 0$ and $= 1$ are found to be 3.9 and 2.9 D, respectively. From the following results even this can be further narrowed down to only the conformer MPCC-1-c. Although thermodynamically both the closed forms are equally stable, the solvatochromic results have shown that the μ_e predicted from AM1 calculations for MPCC-2-c form, taking configurational interactions in to account, is too small (2.9 D) in comparison to that of MPCC-1-c (4.8 D) This is further supported by the greater IHB, i.e. reflected by the shorter hydrogen bond distance (0.197 nm) between the hydroxyl proton and the carbonyl group in MPCC-1-c as compared to 0.223 nm between ≻N–H proton and carbonyl group in MPCC-2-c (larger planarity of the ester group with the carbazole moiety) in MPCC-1-c in comparison to MPCC-2-c (Table 1), as well as, the decrease in the hydroxyl stretching frequency to 3390.25 cm^{-1} (Fig. 7).

Having established the presence of only one form of MPCC as MPCC-1-c, following results can be discussed. The agreement between the predicted and the observed values of μ_e are not very good, although it is close to that when isotropic polarizability is taken in to account. Spectral properties of fluorene, carbazole and phenanthrene are quite close to each other [65]. The difference between these molecules is the presence of lone pair of electrons in the p orbital on ≻N–H group. The lone pair of electrons takes part in the intramolecular charge transfer towards the π cloud of the homocyclic rings and thus polarizing the molecule as shown below.

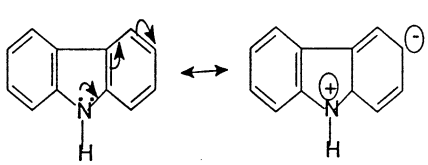

This is supplemented by the: (i) electrophillic substitution occurring at 3-position, favored by 3, 6- and 3, 6, 1- for di- and trielectrophillic substitution; (ii) increase in the pK_a value of 2-hydroxy carbazole [64] (10.5) and decrease in

the pK_a value of >N–H proton. In other words, the increase in the dipole moment of MPCC up on excitation can be nicely expressed when the contribution of the polarizability is considered. Small difference in the μ_e value could be due to the assumption made that the polarizability is isotropic as well as in calculating the Onsager's cavity radius.

Fluorescence decay following single exponential in all the solvents except acetonitrile and methanol and observing similar fluorescence spectrum at different λ_{exc} in all the solvents further prove the presence of only one species, i.e. MPCC-1-c. Double exponential decay observed in acetonitrile and methanol can be explained in the following manner. Even though MPCC-1-o is unstable by 22.5 kJ mol^{-1} in comparison to MPCC-1-c under isolated conditions and the barrier height for the interconversion of these rotamers is 28.7 kJ mol^{-1} in the S_0 state, the presence of polar and protic solvents will favor the equilibrium towards the open structure. In other words, both closed and open structures are present in the system in the S_0 state. Different lifetimes observed also suggest that the equilibrium is not established between the two species in the S_1. It may be mentioned here that the interconversion of these conformers is not possible in the S_1 state as the barrier height increases in the S_1 state from 28.7 to 38.1 kJ mol^{-1}. Fluorescence decays followed at different λ_{em} (360, 400, 440 nm) in these two solvents have shown that the relative amplitude of the short-lived species increases with the increase in the λ_{em}. This suggests that the short-lived species contributes to the red part of the fluorescence spectrum. This is substantiated by the increase in the FWHM of the emission spectrum in polar protic solvents and when TFE was added to cyclohexane (Fig. 12). TFE being stronger hydrogen bonding solvent than ethanol, will shift the equilibrium towards the open structure (MPCC-1-o), followed by an increase in the FWHM and decrease in the ϕ_{fl}. Values of k_{nr} and k_r for these two solvents were calculated using the average value of τ, obtained from the bi-exponential decay. These observations are consistent with the fact that the open structure being more flexible will increase the value of k_{nr} [66], in agreement with the data of Table 4. Decrease in the value of ϕ_{fl} of MPCC in cyclohexane containing TFE further supports that the intermolecular hydrogen bonding plays the major role in the non-radiative decay process than IHB.

It is well established that the ESIPT is observed if: (i) IHB is present between the acidic and basic centers in the S_0 state; (ii) acidity and basicity of the respective center increase on excitation to S_1 state; (iii) ESIPT is an exothermic process in the S_1 state. The first two conditions are present in MPCC-1-c but the conversion of MPCC-1-c to MPCC-1-T is endothermic by 17.5 kJ mol^{-1} in S_1 state (Fig. 4). Although both endothermicity and barrier height for the ESIPT process in S_1 state decrease as compared to those in S_0 state, still these values are so high that this process is not viable in S_1 state at room temperature. The other possible reason could be the presence of close by $n\pi^*$ S_2 state in MPCC tautomer which is separated by only 1500 cm^{-1} (0.186 eV). Due to this, some $n\pi^*$ character will be present in S_1 state and thus enhance the intersystem crossing rate to the $\pi\pi^*$ triplet states. A similar behavior is also observed in many other systems [39–42]. Scheiner's [67] theoretical studies of the excited state proton transfer in small model systems have established that IHB is strengthened and the transfer barrier is reduced in $^1\pi\pi^*$ and barrier is increased in $^3\pi\pi^*$ and $^1n\pi^*$ states.

The spectral changes observed in the absorption and fluorescence spectra of MPCC in the basic and acidic conditions are consistent with the structures of the species present under similar environments. The first deprotonation occurs from the hydroxyl group as the deprotonation constants [38] for the aromatic alcohols are at ~10. Red shift observed in the absorption spectrum of MA of MPCC is due to stronger hydrogen bonding between the carbonyl oxygen and >N–H moiety. This may lead to more planar structure of the MA and larger delocalization of the lone pair from the hydroxyl oxygen. Slightly larger value of pK_a for the N–MA equilibrium of MPCC in comparison to aromatic alcohols is due to the presence of IHB (MPCC-1-c). Similar behavior has also been observed in other similar systems [38,68]. In case of DA, the presence of negative charge on the >N$^-$ and on O$^-$ moieties compel the ester group to be out of plan with carbazole moiety, leading to the loss of the overlap of the π cloud of the carbazole and ester moiety and thus blue shift in the absorption and fluorescence spectra of DA in comparison to MA and neutral carbazole. Ground state pK_a values observed from the fluorometric titration method for the N–MA and MA–DA equilibriums indicate that these equilibriums were not established in the S_1 state and could be due to the faster radiative decay rates of the respective conjugate acid–base pairs. pK_a^* (2.3) value obtained for the MC–N equilibrium suggested that the carbonyl group becomes stronger base in the S_1 state as observed by others [38]. This is further supported by: (i) observation of MC fluorescence band in cylclohexane containing 1 M TFA when no change has been noticed in the absorption spectrum of the neutral MPCC, and, (ii) potential energy mapping (not shown) has also shown that the reactivity of the neutral MPCC towards protonation at the carbonyl oxygen increases from 221 kJ mol^{-1} in S_0 state to 283.4 kJ mol^{-1} S_1 state.

6. Conclusions

The above study leads to the following conclusions: (i) all the transitions in MPCC are of $\pi\pi^*$ in nature; (ii) LW absorption band of carbazole is affected by IHB between the carbonyl and hydroxyl proton; (iii) intermolecular hydrogen bonding and polarity of the solvents are predominant in the non-radiative decay of the excited molecules in S_1 state; (iv) ESIPT process is endothermic even in the S_1 state and is not viable at room temperature. The other reason could be the presence of close by $n\pi^*$ S_2 state in MPCC, which is separated by ~1500 cm^{-1}.

Acknowledgements

The authors are thankful to the Department of Science and Technology, New Delhi for the financial support to the project no. SP/SI/H-07/2000.

References

[1] L.G. Arnaut, S. Formosinho, J. Photochem. Photobiol. A: Chem. 75 (1993) 21.
[2] S.M. Ormson, R.G. Brown, Prog. React. Kinet. 19 (1994) 45.
[3] D. Legourrieve, S.M. Ormson, R.G. Brown, Prog. React. Kinet. 19 (1994) 211.
[4] M. Kasha, J. Chem. Soc., Faraday Trans. 2 (82) (1986) 2379.
[5] M. Wiechmann, H. Port, W. Frey, F. Larmer, T.J. Elsaesser, J. Phys. Chem. 95 (1991) 1918.
[6] H. Eisenberger, B. Nickel, A.A. Ruth, A.W. Al-Soufi, K.H. Grellmann, M. Novo, J. Phys. Chem. 95 (1991) 10509.
[7] F. Rodriguez-Prieto, M.C.R. Rodriguez, M.M. Gonzale, M.A.R. Fernandez, J. Phys. Chem. 98 (1994) 8666.
[8] A. Douhal, F. Amat-Guerri, U. Acuna, J. Phys. Chem. 99 (1995) 76.
[9] A. Douhal, F. Lahanami, A.H. Zewail, Chem. Phys. 207 (1996) 477.
[10] M. Brauer, M. Mosquera, J.L. Perez-Lustres, F. Rodriguez-Prieto, J. Phys. Chem. 102 (1998) 10736.
[11] C. Chudoba, E. Riede, M. Pfeiffer, T. Elsaesser, Chem. Phys. Lett. 263 (1996) 622.
[12] M.C.R. Rodriguez, F. Rodriguez-Prieto, M. Mosquera, Phys. Chem. Chem. Phys. 1 (1999) 253 (and references listed there in).
[13] M. Mosquera, J.C. Penedo, M.C.R. Rodriguez, F. Rodriguez-Preito, J. Phys. Chem. 100 (1996) 5398.
[14] E. Caldin, V. Gold, Proton Transfer Reactions, Halsted Press, New York, 1975, p. 448.
[15] R. Stewart, The Proton: Applications to Organic Chemistry, Academic Press, Orlando, FL, p. 1985.
[16] S. Scheimer, Acc. Chem. Res. 18 (1992) 174.
[17] P. Chou, D. McMorrow, T.J. Aartsma, M. Kasha, J. Phys. Chem. 88 (1984) 4596.
[18] P.F. Barbara, P.K. Walsh, L.E. Bruss, J. Phys. Chem. 93 (1989) 29.
[19] M.L. Ferrer, A.U. Acuna, F. Amar-Gurei, A. Costela, J.M. Figuera, F. Florido, R. Sastre, Appl. Opt. 33 (1994) 2266.
[20] M. Liphano, A. Goonesekera, B.E. Jones, S. Ducharme, J.M. Takoes, L. Zhang, Science 263 (1994) 367.
[21] A. Douhal, R. Sastre, Chem. Phys. Lett. 219 (1994) 91.
[22] M.L. Martinej, W.C. Cooper, P.T. Chou, Chem. Phys. Lett. 193 (1992) 151.
[23] D.L. Williams, H.S. Hellar, J. Phys. Chem. 74 (1970) 4473.
[24] H.J. Hellar, H.R. Blattmann, Pure Appl. Chem. 36 (1973) 141.
[25] T. Werner, G. Woessener, H.E.A. Kremer, in: S.P. Pappas, F.H. Winslow (Eds.), Photodegradation and Photostbilization of Coating, American Chemical Society, Washington, DC, 1981, p. 1511.
[26] T. Werner, J. Phys. Chem. 83 (1979) 320.
[27] R.M. Tarkka, X. Zhang, S.A. Jenekhe, J. Am. Chem. Soc. 118 (1996) 9438.
[28] R. Das, S. Mitra, D. Nath, S. Mukherjee, J. Phys. Chem. 100 (1996) 14514.
[29] A. Sytnik, J.C. del Valle, J. Phys. Chem. 99 (1995) 13028.
[30] A. Sytnik, M. Kasha, Proc. Natl. Acad. Sci. U.S.A. 91 (1994) 8627.
[31] A. Sytnik, I. Litvinyuk, Proc. Natl. Acad. Sci. U.S.A. 93 (1996) 12959.
[32] A. Douhal, Science 227 (1997) 221 (and references listed therein).
[33] A. Douhal, F. Lahamani, A. Zehnacker-Rentien, F.A. Amat-Gueri, J. Phys. Chem. 98 (1994) 12198.
[34] S.I. Lee, J.D. Jang, J. Phys. Chem. 99 (1995) 7537 (and references listed therein).
[35] S. Santra, G. Krishnamoorthy, S.K. Dogra, Chem. Phys. Lett. 311 (1999) 55.
[36] S. Santra, G. Krishnamoorthy, S.K. Dogra, Chem. Phys. Lett. 327 (2000) 230.
[37] S. Santra, G. Krishnamoorthy, S.K. Dogra, J. Phys. Chem. 104 (2000) 476 (and references listed there in).
[38] J.F. Ireland, P.A.H. Wyatt, Adv. Phys. Org. Chem. 12 (1976) 443.
[39] T.P. Carter, M.H. Van Bentham, G.D. Gillispie, J. Phys. Chem. 87 (1983) 1891.
[40] T.P. Carter, G.D. Gillispie, M.A. Connolly, J. Phys. Chem. 86 (1982) 192.
[41] G. Sanlulevich, A. Amirav, U. Even, J. Jortner, J. Chem. Phys. 73 (1982) 1.
[42] M.K. Nayak, S.K. Dogra, unpublished results.
[43] B.S. Furniss, A.S. Hunafols, V. Rogers, P.W.G. Smith, A.R. Talchell, Vogel's Text Book of Practical Organic Chemistry, ELBS, London, 1980, p. 755.
[44] J.A. Riddick, W.B. Bunger, Organic Solvents, Wiley/Interscience, New York, 1970.
[45] G. Krishnamoorthy, S.K. Dogra, J. Org. Chem. 64 (1999) 6566.
[46] G.G. Guilbault, Practical Fluorescence, Marcel-Dekker, New York, 1973, p. 13.
[47] H. Hinze, H.H. Jaffe, J. Am. Chem. Soc. 84 (1962) 540.
[48] M.J.S. Dewar, E.G. Zoeblish, E.F. Healy, J.P. Stewart, J. Am. Chem. Soc. 107 (1985) 3902.
[49] S. Santra, S.K. Dogra, Chem. Phys. 226 (1998) 285.
[50] T. Arthen-Engeland, T. Bultmann, N.P. Earnsting, M.A. Roderiguez, W. Theil, Chem. Phys. 163 (1992) 43.
[51] J. Catalan, F. Fabero, M.S. Guijarro, R.M. Clarament, M.D. Santa Maria, M. dela Concepcion Foces-Foces, F.H.J. Cano, R.S. El, J. Am. Chem. Soc. 112 (1990) 746.
[52] B. Dick, J. Phys. Chem. 94 (1990) 5752.
[53] P. Purkayastha, N. Chattopadhyay, Phys. Chem. Chem. Phys. 2 (2000) 203.
[54] N. Mataga, T. Kubata, Molecular Interactions and Electronic Spectra, Marcel-Dekker, New York, 1970.
[55] J.F. Letard, R. Lapouyade, W. Rettig, Chem. Phys. Lett. 222 (1995) 209.
[56] E. Lippert, Z. Electrochem. 61 (1957) 962.
[57] A. Kawasaki, F. Rabek (Eds.), Progress in Photochemistry and Photophysics, vol. 5, CRC Press, Boca Raton, FL, 1992, p. 2 (and references listed therein).
[58] E. Lippert, Z. Naturforch. 10A (1955) 541;
E. Lippert, Z. Naturforch. 17A (1955) 621.
[59] N. Mataga, Y. Kaifu, M. Koizumi, Bull. Chem. Soc. Jpn. 28 (1955) 690.
[60] M.B. Ledger, P. Supan, Spectrochim. Acta A 23 (1967) 3007.
[61] R.S. Moog, N.A. Burozski, M.M. Desai, W.R. Good, C.D. Silvers, P.A. Thompson, J.D. Simon, J. Phys. Chem. 95 (1991) 8466.
[62] R. Manoharn, S.K. Dogra, J. Photochem. Photobiol. A: Chem. 50 (1989) 53.
[63] G.E. Johnson, J. Phys. Chem. 78 (1974) 1512.
[64] M. Krishnamoorthy, S.K. Dogra, Spectrochim. Acta A 42 (1986) 793.
[65] H.H. Jaffe, M. Orchin, Theory and Applications of Ultraviolet Spectroscopy, Wiley, New York, 1970, p. 356.
[66] G. Kohler, J. Photochem. 38 (1987) 217.
[67] S. Scheiner, J. Phys. Chem. A 104 (2000) 5898.
[68] M. Krishnamurthy, S.K. Dogra, J. Photochem. 32 (1986) 235.